Zinc Oxysulfide Thin Films Grown by Atomic Layer Deposition

B. W. Sanders

Institute for Environmental Chemistry, National Research Council, Ottawa, Ontario, Canada K1A 0R6

A. Kitai*

Department of Materials Science and Engineering, McMaster University, Hamilton, Ontario, Canada L8S 4K6

Received January 15, 1992. Revised Manuscript Received May 11, 1992

The chemical vapor atomic layer deposition technique was used to deposit thin films of $ZnO_{1-x}S_x$ on glass and silicon substrates. Film composition was varied from $x = 0$ to $x = 0.95$, and measurements of bandgap and resistivity yielded surprising minima at $x \sim 0.6$. Results of Rutherford backscattering, X-ray, and luminescence measurements are also presented. Both one- and two-phase films are visible in scanning electron microscopy, and an amorphous phase is also apparent. A continuously variable mixed film is not observed due to the large lattice mismatch between ZnO and ZnS.

Introduction

The most successful thin-film electroluminescent displays produced to date have used manganese-doped zinc sulfide as the phosphor layer. Thin films of ZnS prepared by chemical vapor deposition,[1] sputtering,[2] and evaporation[3] contain significant amounts of oxygen. Surprisingly, there have been few studies of the effect of oxygen on the properties of zinc sulfide. The one study performed did not determine the oxygen content of the films.[4] The present study has determined some properties of zinc oxysulfide films.

Thin films of $ZnO_{1-x}S_x$ ($0 \leq x \leq .95$) were grown on silicon and Corning 7059 glass using chemical vapor atomic layer deposition (CVALD). Depending on the value of x, these mixed films have properties similar to ZnO and ZnS or that are unique to the film mixture. The method of CVALD was chosen because of its good control over the film deposition.[5-7] The thickness of the film can be monitored by counting the number of growth cycles. Since the film is grown one monolayer at a time, good uniformity is obtained throughout the film. The growth of these films is not restricted to the reactant materials used in this study. A wide range of chemical precursors[8] could be used to deposit thin films of $ZnO_{1-x}S_x$ by slightly modifying the growth parameters.

Experimental Section

Films of $ZnO_{1-x}S_x$ were deposited on Corning 7059 glass, or single-crystal n-type (111) silicon (from MEMC materials) substrates. Each substrate measured approximately 2 cm by 2 cm. The cleaning procedure differed for each substrate type. The glass substrates were ultrasonicated in a surfactant solution for 2 min, rinsed in deionized water for 1 min, and ultrasonicated for 2 min in isopropyl alcohol. They were then allowed to air dry.

Silicon substrates were cleaned by a slightly modified form of the standard RCA cleaning method[9,10] prior to deposition. The substrates were first immersed in a 75–80 °C solution consisting of high-purity water, 30% hydrogen peroxide, and ammonium hydroxide in the ratio 5:1:1 for 10 min. They were then rinsed three times with high-purity water. Next, the wafers were immersed in a 75–80 °C solution consisting of high-purity water, 30% hydrogen peroxide, and hydrochloric acid in the ratio 6:1:1. After rinsing three times with high-purity water, the samples were blown dry with nitrogen.

Table I. Deposition Parameters for Growth of $ZnO_{1-x}S_x$ Films

deposition parameter	value
nitrogen flush pressure	50 PSIG
dimethylzinc cylinder pressure	50 PSIG
hydrogen sulfide cylinder pressure	30, 50 or 70 PSIG
dimethylzinc reaction time	2 s
hydrogen sulfide reaction time	5 s
nitrogen purge time	11 s at a standard flow rate of 1 L/min
delay to allow nitrogen back-pressure to drop	0–8 s

Films of $ZnO_{1-x}S_x$ were deposited using dimethylzinc, 1% hydrogen sulfide in nitrogen, and the trace oxygen and/or water present (up to 2 ppm) in ultrahigh-purity (UHP) nitrogen. The dimethylzinc was contained in a stainless steel cylinder equipped with a dip tube (supplied by Strem Chemicals). To lower the dimethylzinc vapor pressure, the cylinder was held at 273 K using an ice water bath. Prepurified nitrogen (Canada Liquid Air) served as a carrier gas for the dimethylzinc. Gas pressures are given in Table I. A description of the deposition system and its operation follows.

The deposition system is schematically illustrated in Figure 1. It uses a computer-controlled 12-position valve (Valco Inc.) with electric actuator, a 2-position valve (Valco Inc.) with an air actuator and four air-operated bellows valves. The 12-position valve is responsible for selecting the appropriate reactant gas as the deposition proceeds. The 2-position valve controls whether the selected gas stream is trapped or admitted to the reaction chamber.

Substrates were placed in the reaction chamber illustrated in Figure 2. The heated region was circular and had a diameter of 3.7 cm. A chromel–alumel thermocouple was placed at the junction of the copper block and the chamber to monitor the substrate temperature. The temperature was controlled using a resistance heater and a temperature controller. This chamber allows for good conservation of source materials because of its small volume (3.5 cm^3). All source gases pass over the substrate on their way through the chamber, further promoting the eco-

(1) Hunter, A. Deposition of Zinc Sulphide Thin Films Using Organometallic Atomic Layer Epitaxy. M.Sc. Thesis, McMaster University, Hamilton, Ontario, Candada, 1987.
(2) Blackmore, J. M.; Blackmore, G. W.; Dosser, O. D.; Slater, M. J. *Thin Solid Films* **1990**, *192*, 321.
(3) Banovec, A.; Stariha, B.; Zalar, A.; Pracek, B.; Kern, M. *Vacuum*, **1990**, *41*, 1437.
(4) Qiu, S. N.; Qiu, C. X.; Shih, I. *Can. J. Phys.* **1989**, *67*, 435.
(5) Herman, M. A. *Vacuum* **1991**, *42*, 61.
(6) Goodman, C. H. L.; Pessa, M. V. *J. Appl. Phys.* **1986**, *60*, R65.
(7) Suntola, T.; Hyarvinen, J. *Annu. Rev. Mater. Sci.* **1985**, *15*, 1977.
(8) Leskela, M. Atomic Layer Epitaxy in the Growth of Polycrystalline and Amorphous Films. In *Acta Polytech. Scan., Chem. Tech. Met. Ser.* **1990**.
(9) Kern, W. *J. Electrochem. Soc.* **1990**, *137*, 1887.
(10) Kern, W.; Poutinen, D. *RCA Rev.* **1970**, *31*, 187.

0897-4756/92/2804-1005$03.00/0

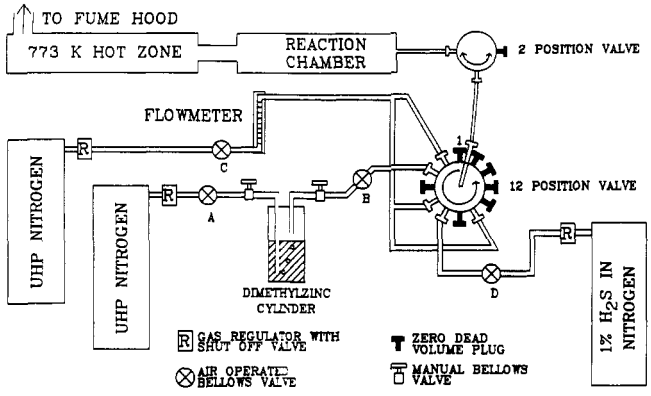

Figure 1. Deposition system. Controlled amounts of zinc, sulfur, and oxygen are introduced to the reaction chamber in a sequential manner by computer-controlled bellows valves and multiposition valves.

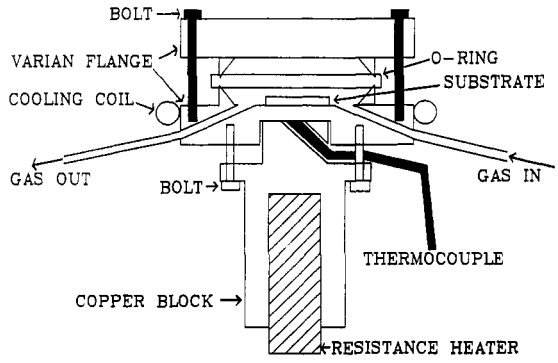

Figure 2. Deposition chamber. The chamber uses two Varian 2-$^3/_4$-inch conflat flanges (one was modified to allow entry and exit of the reactant gases), a copper heating block, and water coolings coils. The bottom flange was thinned in the region of the copper block to provide better heat conduction to the substrate.

nomical use of source material.

Films are grown in a stepwise fashion under computer control (a listing of deposition parameters is given in Table I). First, a volume (20.3 μL) of DMZ is trapped under pressure in the narrow tube between the 2- and 12-position valves. This volume is then allowed to expand into the chamber and react with the heated substrate. The 12-position valve is rotated and the chamber is purged with nitrogen. The 2-position valve closes. The trapping volume is filled with hydrogen sulfide. The H_2S is then allowed to expand into the reaction chamber where it reacts with the growing film. This pattern is repeated until the required number of growth cycles are completed (10–2000 cycles were typically used). Growth chamber pressure is 1 atm, slightly higher during gas admission.

The following analysis procedures were applied to films grown by CVALD. All measurements were performed at room temperature.

UV–visible absorption spectra of as grown films were obtained on a Hewlett-Packard diode-array spectrophotometer over an area of 1 cm^2. Scanning Auger spectra were recorded over an area of 40 μm^2 of the film surface using a Perkin-Elmer PHI 600 Auger spectrometer. Auger signal normalization was performed using sensitivity factors obtained from a zinc sulfide single crystal, instead of the internal standards present with the system. Powder X-ray diffraction was performed on a Nicolet diffractometer over an area of 2 mm^2. Film thickness measurements were performed on a Tencor Alpha Step stylus type instrument. Electron micrographs were performed on a Phillips Model SEM 515 scanning electron microscope.

Cathodoluminescence spectra were collected under a vacuum of at least 1×10^{-7} Torr. A Perkin-Elmer electron gun served as the electron source. Spectra were collected at either 4 or 5 eV over an area of approximately 1 mm^2 using a 0.25-m monochromator.

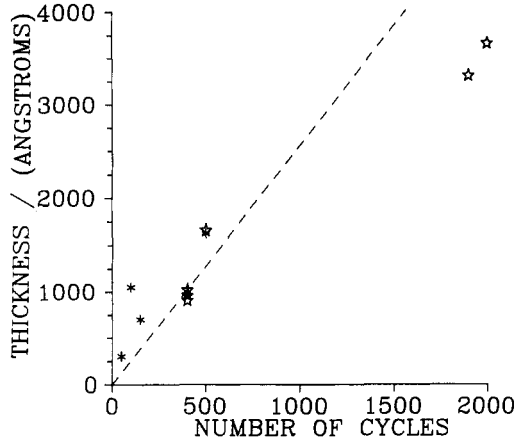

Figure 3. Growth rate of ZnO. Thickness of film measured with a mechanical profilometer as a function of the number of growth cycles. The dashed line shows the theoretical values for one layer per cycle of ZnO in the [111] direction. Growth at (asterisks) 200 °C and (open stars) 300 °C. Dashed line: ideal growth, 2.56 Å/cycle.

Rutherford backscattering spectra were collected using the KN accelerator at McMaster University. ^{4}He atoms with incident energies of 2 MeV were used. The target current was 10 nA. The detector angle was 160°. Data collection proceeded until 40 μC were collected. Spectra were collected over an area of 0.6 mm^2. Some spectra of $ZnO_{1-x}S_x$ films grown on silicon were collected when the substrate was under a channeling condition. This allowed for better definition of the oxygen peak which sits on the silicon background. Hall measurements were performed using indium contacts.

Results and Discussion

Thin-Film Growth. The growth of ZnO films is easily accomplished in this system. First, a small volume of dimethylzinc (DMZ) and nitrogen mixture is trapped between the 2-position and 12-position valves. This volume is then allowed to expand into the reaction chamber and adsorb or react on the substrate. A subsequent flush with nitrogen gas oxidizes the DMZ (due to the trace impurities) on the surface of the substrate. Another volume of dimethylzinc vapor is trapped and the process repeats. Close to one monolayer growth per reaction cycle is realized. Figure 3 compares the actual thickness of ZnO grown as a function of number of reaction cycles to the ideal case.

The growth of zinc sulfide is slightly more complicated. The zinc oxide film first formed must be converted to zinc sulfide by hydrogen sulfide. This reaction does proceed readily.[11] In practice, zinc sulfide is not obtained with a 30 psig hydrogen sulfide pressure. Pressures of up to 70 psig are required to obtain zinc sulfide films of reasonable stoichiometry (Figure 4).

The reason becomes apparent when the system operation is examined. If the 2-position valve is closed before the nitrogen purge is stopped, the trapped volume will contain a volume of gas at a pressure equal to the flushing pressure (50 psig). When an attempt is made to introduce the H_2S at 30 psig, there is a net flow of gas out of, not into, the trapped volume. This results in no hydrogen sulfide reaching the substrate. To alter this situation, a delay is introduced between the time the nitrogen flush is terminated and the 2-position valve closed. This allows the nitrogen back pressure to drop to 1 atm. By changing the hydrogen sulfide pressure and the time allowed for the back pressure to release, varying amounts of H_2S can be

(11) Westmoreland, P. R.; Gibson, J. B.; Harrison, D. P. *Environ. Sci. Technol. 11*, 488.

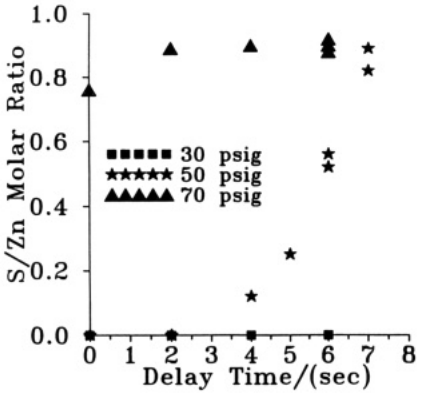

Figure 4. Film composition as a function of delay time. Films vary in composition from ZnO to $ZnO_{0.1}S_{0.9}$. Indicated pressures refer to the 1% H_2S in N_2 gas pressure.

admitted to the chamber. This theoretically offers the possibility of producing films of $ZnO_{1-x}S_x$ with x varying from 0 to 1. In practice it has been possible to produce films in which x varies from 0 to 0.95. The value of x in Figure 4 is limited to 0.9 because of reoxidation of the ZnS by the oxygen contained in the purge gas. Rao and Kumar[12] have shown that oxidation of ZnS does occur below 873 K. To increase the value of x above 0.9, one must reduce the concentration of oxygen in the flushing gas. This can be accomplished by passing the nitrogen through an oxygen trap. The oxygen trap reduces the oxygen content to 25 ppb by volume. With this trap in place, S:Zn ratios of 0.95 were obtained.

Film Properties. Thin films of ZnS and ZnO ranging in thickness from 300 to 5000 Å have the morphology shown in Figure 5. Each covers the substrate uniformly. The ZnS films have a very different surface structure from ZnO films. ZnS films exhibit more circular grains compared to ZnO films. The grain size of a ZnS film grown at 573 K to a thickness of 1000 Å is 1000 Å. This is greater than the grain size of 300 Å reported for ZnS thin films grown by a similar technique.[13]

It was not feasible to perform Auger analysis on these thin films because of charging problems. Only Rutherford backscattering analysis was performed. Figure 6 is a Rutherford spectrum of a zinc sulfide film growth on silicon at 573 K. A quantitative analysis of the data gives an average S:Zn ratio of 0.9 without an oxygen filter and a ratio of 0.95 with an oxygen filter present.

No oxygen peak is visible in the Rutherford spectrum; the presence of oxygen is only implied by the nonstoichiometry exhibited between the sulfur and the zinc. When a significant oxygen peak was present, Rutherford analysis gave O + S:Zn ratios equal to 1:1. The sensitivity of this technique to oxygen is very low compared to its sensitivity to silicon.

Powder X-ray diffraction performed on ZnS films (Figure 7) indicates they grow predominantly in a cubic ⟨111⟩ or hexagonal ⟨002⟩ direction. The lack of any other peaks precludes determination of whether the films are cubic or hexagonal in nature.

The films are transparent to light in the visible range of the spectrum (Figure 8). The transmission data can be used to determine the bandgap of the film. Using the familiar relationship between absorbance and transmittance ($A = -\log T$) the absorbance of the films can be calculated from the transmission data. Using the equation $(Ah\nu)^2 = C(h\nu - E_g)$[17] the bandgap of the film, E_g, can be

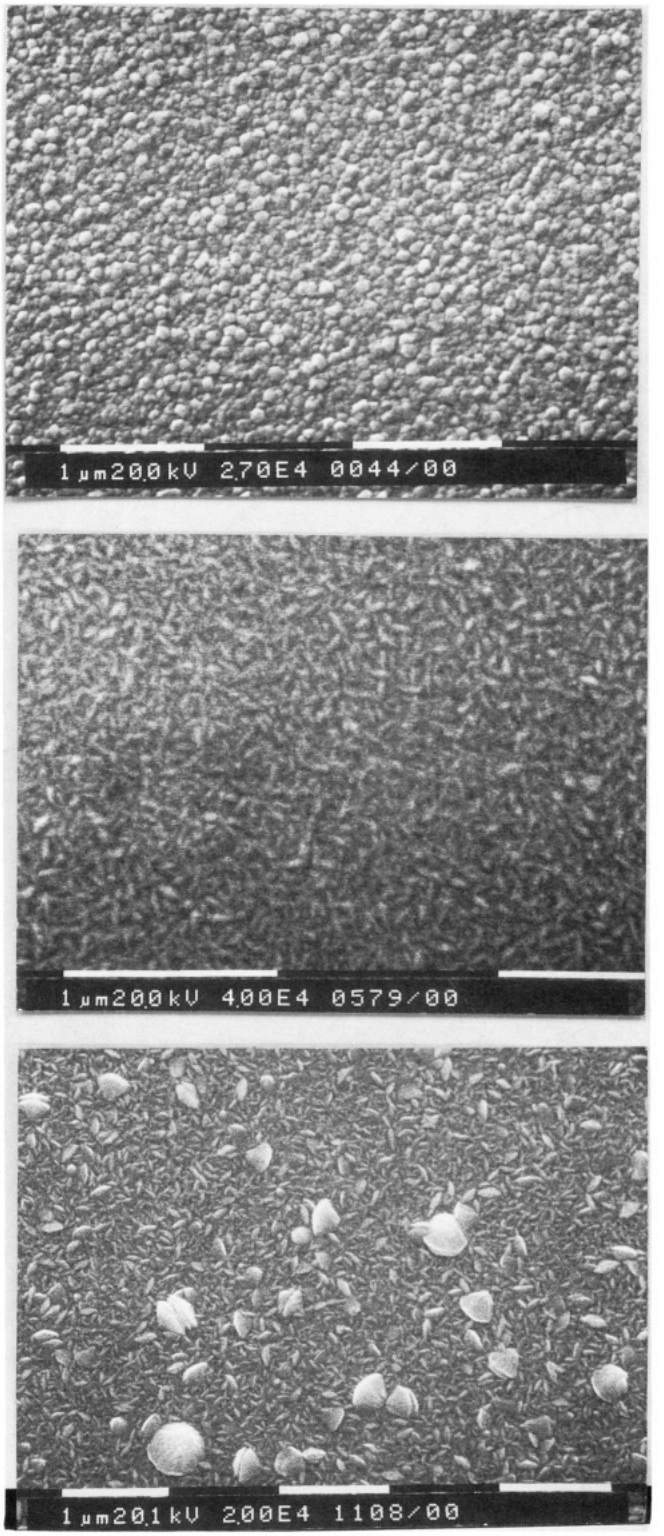

Figure 5. Electron micrographs of $ZnO_{0.1}S_{0.9}$ thickness 1000 Å (a, top), ZnO thickness 300 Å (b, middle), and ZnO thickness 1000 Å (c, bottom).

obtained as the x intercept of a plot of $(Ah\nu)^2$ vs $h\nu$. (The h, ν, and C in the equation are Planck's constant, frequency, and a constant, respectively). The bandgap obtained from these data is 3.58 eV, which is close to the value of 3.65 eV reported in the literature.[14] The lower value may be due to oxygen contamination. The tran-

(12) Rao, T.; Kumar, R. *Chem. Eng. Sci.* **1981**, *37*, 987.
(13) Hunter, A.; Kitai, A. H. *J. Cryst. Growth* **1988**, *91*, 111.
(14) Hartman, H.; Mach, R.; Selle, B. *Wide Gapp II-VI Compounds as Electronic Materials, in Current Topics in Materials Science*; (Kaldis, E., Ed.; North-Holland: Amsterdam, 1982; Vol. 9.

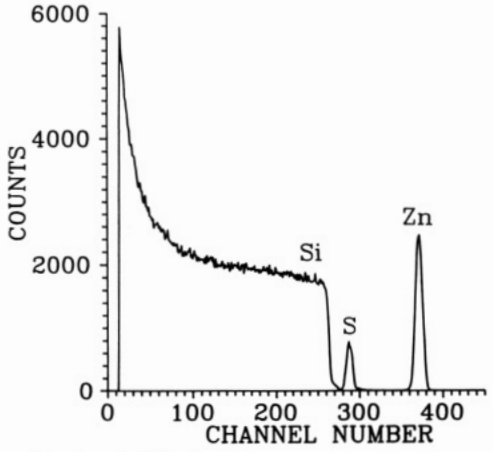

Figure 6. Rutherford backscattering spectrum of ZnS film on silicon at 573 K.

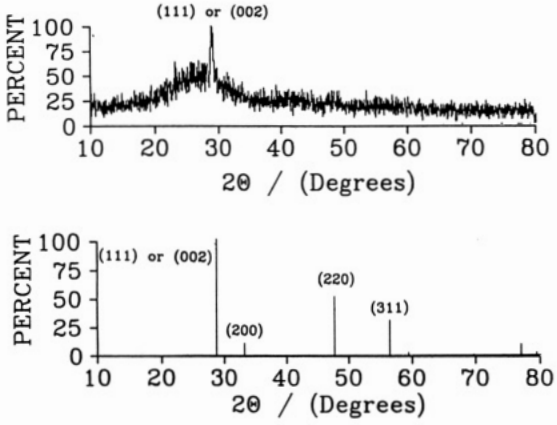

Figure 7. Powder X-ray diffraction pattern of ZnS film grown on glass. The standard peaks for cubic ZnS powder are shown below. The (002) planes are for a hexagonal lattice.

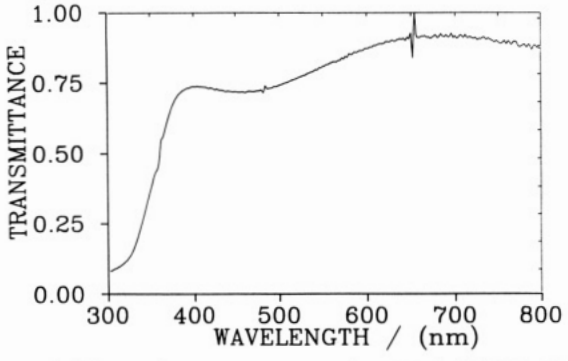

Figure 8. Transmittance spectrum of a 1000-Å-thick ZnS film grown on Corning 7059 glass.

sparency of these films makes them desirable for use in thin film phosphors.

A typical Rutherford spectrum of a mixed (x = 0.55) $ZnO_{1-x}S_x$ thin film is shown in Figure 9. The spectrum clearly shows the presence of Zn, S, O, and a signal from the silicon substrate.

Scanning electron micrographs of films with values of x close to 0 or 0.9 indicate that the films have microstructures similar to the parent material (either ZnO or ZnS). Scanning electron micrographs of films of intermediate composition are very different. Figures 10a and 10b are scanning electron micrographs of films with x values of 0.1 and 0.55, respectively. Each exhibits some blackened areas on the surface that do not appear in pure ZnO or ZnS films. Difficulty in obtaining a higher resolution micrograph was encountered as the "islands" disappear under the electron beam within a matter of minutes. This effect can be noticed in the center of Figure 10a, where the islands have faded compared to those on the perimeter. The central region was used for focusing and had a higher electron flux.

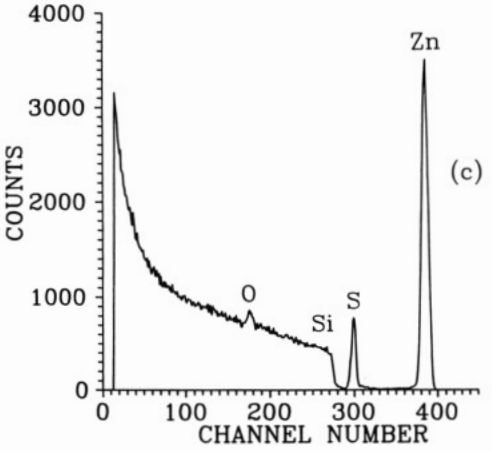

Figure 9. Rutherford backscattering spectrum of ZnO_xS_{1-x} mixed film. Note the presence of the silicon background that is now lower than that of Figure 6 due to the use of channelling.

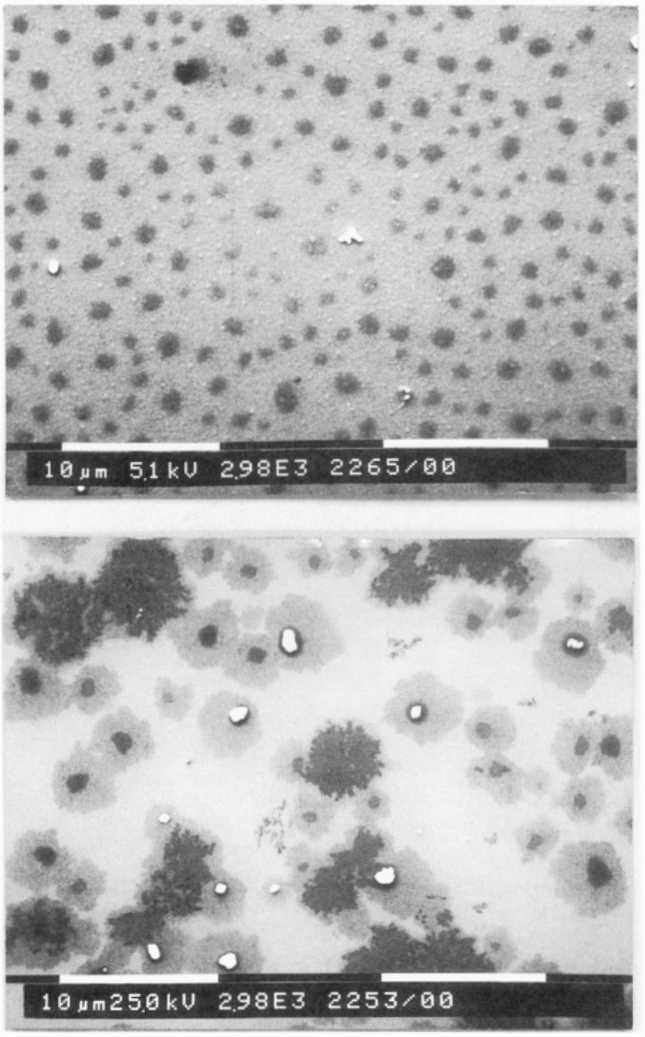

Figure 10. Electron micrographs of $ZnO_{0.9}S_{0.1}$ (a, top) and $ZnO_{0.45}S_{0.55}$ (b, bottom).

Auger analysis of these blackened areas was performed to ascertain their composition. The islands contained a large amount of carbon (>50% in a quantitative analysis).

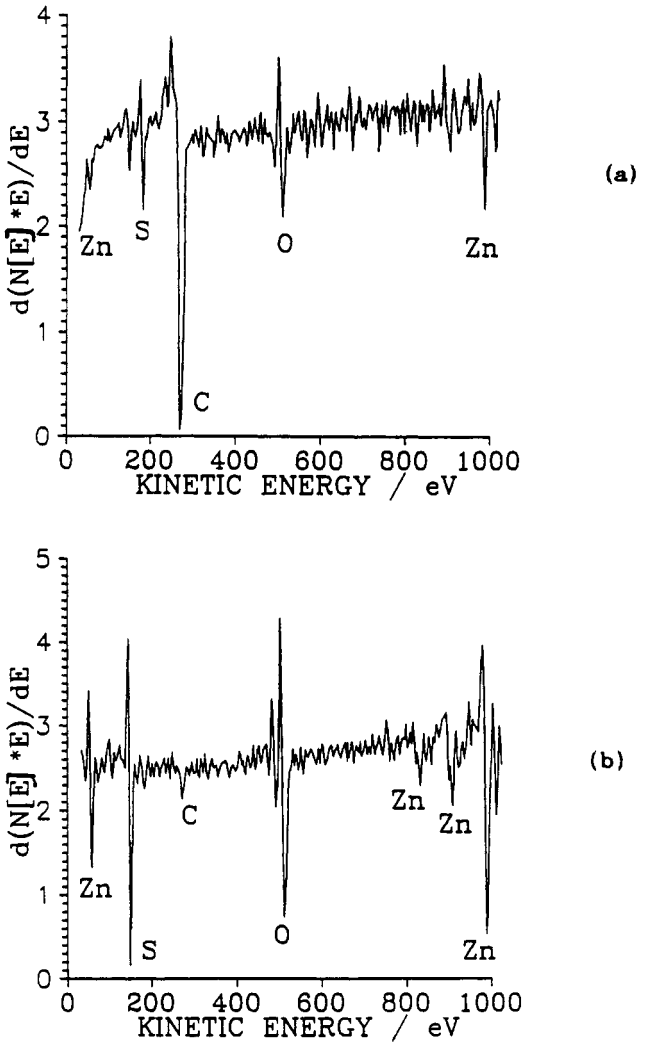

Figure 11. Auger spectra of black areas of mixed film before (a) and after (b) sputtering for a few seconds.

Even the smallest amount of sputtering with an Ar ion beam (10 s at 3 keV) resulted in removal of the islands. The underlying area contained little carbon and appeared homogeneous with the surrounding matrix. Thus, these islands must be the result of incomplete reaction of the dimethylzinc under the conditions of mixed film growth. These points are illustrated by Figure 11. Figure 11a is an Auger analysis of one black region before sputtering. The carbon peak dominates the differentiated spectrum. After a short sputtering time, the carbon almost completely disappears and S, O, and Zn peaks dominate (Figure 11b). Higher deposition temperatures may rid the film of this carbon. At this time the system is limited to 573 K deposition temperature.

Auger analysis of the grey areas in Figure 11b show these areas contain double the S of the lighter areas surrounding them. This indicates the film has a two-phase structure. The two-phase structure of a film of this composition is supported by X-ray diffraction patterns.

Powder X-ray diffraction patterns of films of various compositions are shown in Figure 12. The major peak in Figure 12a,b is smaller than that of a pure film of the same thickness. It is known that as oxygen is added to zinc sulfide the (111) peak begins to disappear. The films become completely amorphous[15] for $0.3 \leq x \leq 0.5$. When the x value reaches 0.56, the X-ray pattern shows ZnO and

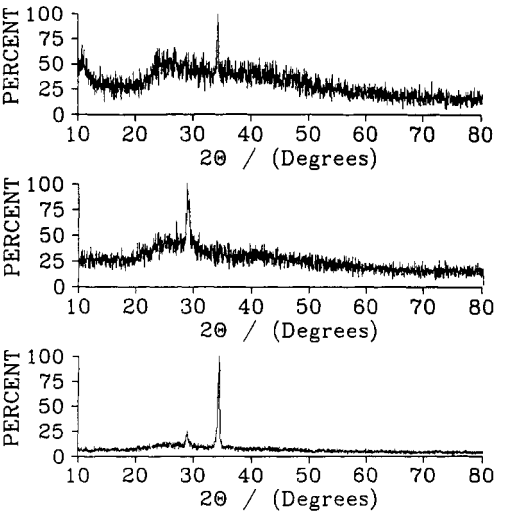

Figure 12. X-ray diffraction patterns of (a) $ZnO_{0.88}S_{0.12}$ (b) $ZnO_{0.34}S_{0.66}$ and (c) $Zn_{0.44}S_{0.56}$, showing how films may be one or two phase.

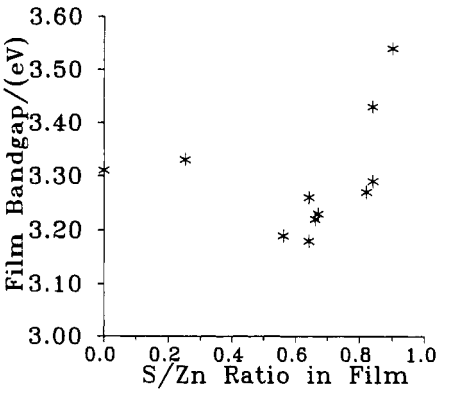

Figure 13. Bandgap measurements as a function of film composition. These results were obtained using optical absorption measurements and show a bandgap minimum at $x \approx 0.65$.

ZnS peaks indicating the film has separated into a two-phase structure. This is not surprising since the lattice constants for hexagonal zinc sulfide and zinc oxide differ by 16%. The strain involved in keeping one phase is too great, so the film separates into a two-phase structure. Qiu et al.[4] also reported that a two-phase film appeared for a small composition range in mixed $ZnO_{1-x}S_x$ films.

The absorbance characteristics of these mixed films exhibit anomalous behavior with composition compared to other II–VI alloys. With films such as $ZnS_{1-x}Se_x$, a continuous and almost linear variation in bandgap from that of pure ZnS to pure ZnSe occurs.[16] With $ZnO_{1-x}S_x$, a minimum in the bandgap versus composition plot is obtained (Figure 13). This behavior has been reported by Qiu et al.[4] Direct comparison of their results with this study is impossible as they sputtered the films and reported only target and not film compositions. The bandgap versus composition curve follows the crystallinity of the film. As the amount of oxygen in the film increases, the bandgap decreases. This is due not only to a change in chemical composition but also because of decreased crystallinity. Just over the halfway point (in composition) the film becomes two-phase and the bandgap is at a minimum. Further increases in oxygen content create a

(15) Takabayashi, A.; Iida, S. *Jpn. J. Appl. Phys.* **1986**, *25*, L437.

(16) Kukimoto, H. *J. Cryst. Growth* **1991**, *107*, 637.

(17) Johnson, E. J. *Absorption Near the Fundamental Edge in Semiconductors and Semimetals*, Willardson, R. K., Beer, A. C., Eds.; Academic Press: New York, 1967; Vol. 3.

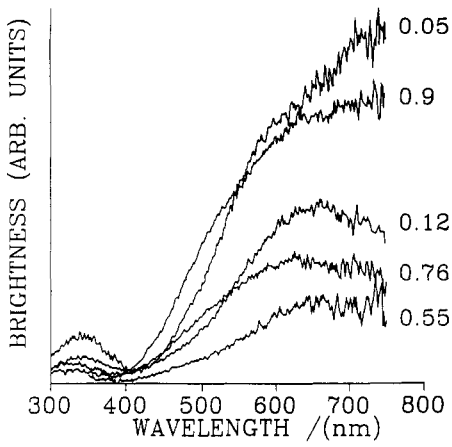

Figure 14. Cathodoluminescence spectra of $ZnO_{1-x}S_x$ films. The number on each curve is the value of x for that measurement. Note that the spectra are similar in shape but differ in intensity.

Table II. Resistivity, Mobility, and Carrier Concentration Results from Hall Measurements Made on the Mixed Films of Figure 15

x in $ZnO_{1-x}S_x$	resistivity, Ω cm	donor concn, cm^{-3}	mobility, $cm^2/V\ s$
0	0.0048	4.8×10^{19}	13.2
0.25	0.101	1.7×10^{18}	36.1
0.56	0.042	1.66×10^{19}	32.2
0.66	1.28	2×10^{17}	24
0.82	8.27	2.4×10^{16}	28
0.92	67.9	2.61×10^{15}	94

more crystalline ZnO-type film with a corresponding increase in bandgap.

Figure 14 shows a series of cathodoluminescent spectra of films with x values ranging from 0.05 to 0.9. All films were in the thickness range 500–700 Å. A broad red peak is present, and a small peak at approximately the gap energy is also seen. The brightness of the red luminescence decreases as the amount of S increases and then increases again once an approximate 50:50 mixture is reached. This suggests that the red emission is tied to the crystallinity of the film.

Hall measurements were performed on $ZnO_{1-x}S_x$ films on glass substrates to determine resistivity, mobility, and carrier concentration. As expected, conductivity was highest in ZnO films. Of significance is that resistivity decreased to a local minimum in films that had a bandgap minimum (Figure 15 and Table II).

Table II demonstrates that the mobility changes little and the main cause of varying resistivity is donor concentration variation. As expected, donor concentration varies inversely with bandgap. The high mobility of the $ZnO_{0.08}S_{0.92}$ film is probably due to the much larger grain size for the high sulfur content films.

The morphology of the films leads to some interesting speculation. As demonstrated by scanning electron microscopy (Figures 5a,b and 10a,b), atomically smooth films do not result from this CVALD technique, perhaps because of the low growth temperature. Films which are predominantly ZnO or ZnS are polycrystalline and homogeneous in nature. In the case of ZnS, the apparent grain sizes are comparable to the film thickness (Figure 5a) as is often the case in the growth of polycrystalline thin films.[18] On the other hand, ZnO films exhibit a textured surface which contains more elongated grains.

The morphology of zinc oxysulfide films resembles more that of ZnS films that ZnO films. This is an interesting

(18) Thompson, C. V. *Annu. Rev. Mater. Sci.* **1990**, *20*, 245.

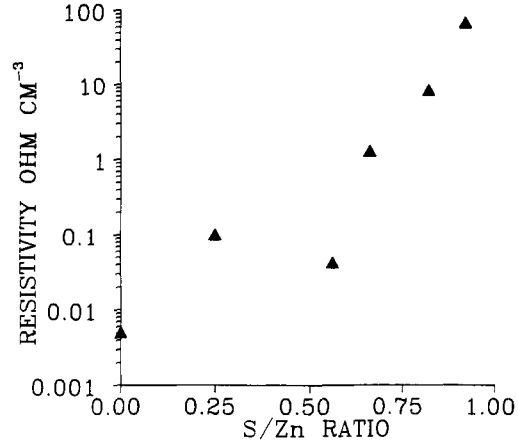

Figure 15. Resistivity of $ZnO_{1-x}S_x$ films showing a local minimum in the mixed films.

observation as the addition of even a small amount of S seems to prevent the elongated grain structure from forming. Also of note are the circular patches which contain more sulfur than the matrix they are embedded in. It is unclear at the moment as to whether these islands extend through the film or are isolated structures. The films could not be sputtered (due to a charging problem) so a compositional depth profile can not be given at this moment. It is still possible to speculate on the nature of the island formation. The lattice constants of ZnO and ZnS vary by 16%. It is not surprising that a two-phase film begins to appear at some point in the sulfation of ZnO. Once a certain sulfur content is achieved, the only way to continue is to begin to form a different phase. This may explain the circular nature of the high sulfur content patches in Figure 10b. Once a spot in the film begins to grow the new high sulfur phase, it continues to grow outward until all the sulfur available to it is exhausted or the next ZnO layer is deposited (i.e., the nucleation and growth of a new phase occurs at the expense of a previous phase). It would be interesting to know if these patches are homogeneous throughout the depth of the film or if they are indeed restricted to a few top layers on the surface.

At the center of many of the patches is a micron-sized particle. The size of this particle is much greater than the film thickness. This might lead one to believe that either the particle's surface offers enhanced growth characteristic through a kinetically faster growth pattern or perhaps these sites preferentially adsorb dimethylzinc.

The questions raised in the preceding paragraphs indicate that the surface chemistry during the film growth is quite complicated. It would prove interesting to investigate the surface chemistry of the deposition process in detail at a later date.

Conclusions

Thin films of $ZnO_{1-x}S_x$ ($0 \le x \le 0.95$) were prepared by atomic layer chemical vapor deposition. The same deposition apparatus was used for all three types of film. The type of film growth depended only on the deposition parameters used.

Thin films of zinc sulfide were produced by ensuring adequate amounts of hydrogen sulfide were admitted to the reaction chamber. An oxygen filter was employed on the nitrogen flush gas to improve the stoichiometry of the films. The bandgap and X-ray diffraction patterns of the films agree well with those in the published literature.

Thin films of $ZnO_{1-x}S_x$ exhibit interesting properties including a minimum bandgap and two-phase structure

in the region of a 50‰ mixture of ZnS and ZnO. Outside the region of a 50:50 mixture the films are amorphous, but they become more crystalline as the stoichiometry approaches either of the pure compounds. The films do not exhibit very bright cathodoluminescence but are of interest as phosphor host materials. As the amount of sulfur increases in the films, the intensity of the red peak decreases and then increases again, following the crystallinity of the film. Resistivity measurements confirm anomalous behavior in the mixed films, possibly associated with amorphous/crystalline phase change.

Acknowledgment. We acknowledge support for the research from the National Science and Engineering Research Council of Canada. We are also indebted to Ms. Doris Stevanovic for help with RBS analysis.

Registry No. ZnO, 1314-13-2; Si, 7440-21-3; $ZnO_{0.05-0.99}S_{0.01-0.95}$, 142395-69-5.

Synthesis and Luminescence Properties of $BaNbOF_5$ with Isolated $[NbOF_5]^{2-}$ Octahedra

A. M. Srivastava* and J. F. Ackerman

GE Corporate Research and Development, Schenectady, New York 12301

Received February 12, 1992. Revised Manuscript Received June 29, 1992

$BaNbOF_5$ has been prepared and characterized by X-ray powder diffraction. It crystallizes in the low-temperature cubic $KSbF_6$ structure with lattice constant $a = 9.893$ Å. Weak reflections in the powder diffraction pattern indicate a deviation from the space group $Ia\bar{3}$, assigned to $KSbF_6$. We comment on the structure of $BaNbOF_5$ and propose $Pa\bar{3}$ as the alternative space group. Efficient blue luminescence is observed for $BaNbOF_5$ and is attributed to the high-energy position of the lowest absorption band. Comparison of luminescence properties is made with those reported for other isolated niobate octahedra.

Introduction

Examples of efficient luminescence from structurally isolated niobate octahedral groups in the literature is rare. Recently, Blasse and Dirksen[1] studied the luminescence of $MgNb_2(P_2O_7)_3$, a compound with no correlation between the niobate octahedra. Their results indicated a low quantum efficiency of luminescence even at 4.2 K. The absence of luminescence from ordered perovskites containing isolated niobium octahedra such as La_2LiNbO_6, $SrLaMgNbO_6$, and Ba_2YNbO_6 was also noted in ref 1. Furthermore, the reasons for efficient luminescence from condensed niobate octahedra and its absence in isolated niobate octahedron has been discussed by Blasse.[2,3] In contrast to these works, we have recently described the efficient room-temperature luminescence of Cs_2NbOF_5, which does contain discrete $[NbOF_5]^{-2}$ octahedral groups.[4] We accounted for its behavior using the single configuration coordinate model for luminescence. There it was shown that small Stokes shifts should not be the only indicator of efficient luminescence for a structurally isolated system, but the excitation energy of the lowest electronic absorption band needs to be considered as well. When a high-energy excitation is present, it is possible to have a large Stokes shift in conjunction with efficient room-temperature luminescence. These conditions could be met in other compounds having isolated oxofluoroniobate octahedra. This possibility initiated our search for structures which could contain such species to determine whether their luminescent properties would be similar to those of Cs_2NbOF_5.

The low-temperature structure of the fluoride $KSbF_6$ has been described in the literature.[5] It also contains isolated MX_6 octahedra with the K^+ ion also in an octahedral 6-coordination. The compound $BaNbOF_5$ could be derived from $KSbF_6$ by making the following substitution:

$$K^+ + Sb^{5+} + F^- \rightarrow Ba^{2+} + Nb^{5+} + O^{2-}$$

Thus, the MX_6 octahedra would then be of the stoichiometry $NbOF_5^{2-}$, identical to that in Cs_2NbOF_5, so that $BaNbOF_5$ would be an excellent candidate for our luminescence search.

Experimental Section

$BaNbOF_5$ was prepared via the dispersion of 0.01 mol of BaF_2 and 0.005 mol of Nb_2O_5 in 500 mL of 25% HF–75% H_2O at 95 °C in a PTFE beaker. The solution was allowed to evaporate to dryness after which an additional 500 mL of acid solution was added and reevaporated. The acid additions were continued until the X-ray diffraction pattern indicated a single phase. The production of a single phase was also indicated by a uniform blue luminescence from the dry product when irradiated with short-wavelength UV light.

A second method of preparation began with the preparation of a mixed phase oxide precursor followed by treating with the HF/H_2O solution. In this method 0.01 mol of $BaCO_3$ was mixed with 0.005 mol of Nb_2O_5 and placed in an alumina crucible. The mixture was then heated to 1100 °C for 12 h and then air quenched. The resulting solid mass ground and refired to 1100 °C for 4 h. After requenching and regrinding, the colorless oxide powder was dispersed in 500 mL of 25% HF–75% H_2O and processed as before. No differences in either the structure or luminescence were seen between samples prepared by these two methods. All materials used are of the highest purity available, ≥99.99%.

Room-temperature X-ray powder diffraction patterns were obtained with a Philips D500 diffractometer calibrated before and after each measurement with pure Silicon. Nominal scan rate of $^1/_4°$ 2θ/min were employed. Refined cell dimensions were obtained by least-squares procedures using a local computer program.

Luminescence excitation and emission spectra were measured at room temperature with a Spex Fluorolog II System, yielding automatically corrected spectra, i.e., the excitation spectra have

(1) Blasse, G.; Dirksen, G. J. *Inorg. Chim. Acta* **1989**, *157*, 141.
(2) Blasse, G. *J. Chem. Phys.* **1968**, *48*, 3108.
(3) Blasse, G.; Bril, A. *J. Phys. Chem. (Munich)* **1968**, *57*, 187.
(4) Srivastava, A. M.; Ackerman, J. F. *Mater. Res. Bull.* **1991**, *26*, 443.
(5) Bode, H.; Voss, E. *Anorg. Allg. Chem.* **1951**, *264*, 144.

0897-4756/92/2804-1011$03.00/0